UNIVERSIDADE FEDERAL DE SANTA CATARINA
PROGRAMA DE PÓS GRADUAÇÃO EM CIÊNCIA E ENGENHARIA DE MATERIAIS

Leandro Neckel

MODELAMENTO E SIMULAÇÃO DE IMPACTO BALÍSTICO EM SISTEMA CERÂMICA-METAL

Dissertação submetida ao Programa de Pós Graduação em Ciência e Engenharia de Materiais da Universidade Federal de Santa Catarina para obtenção do Grau de Mestre em Ciência e Engenharia de Materiais
Orientador: Prof. Hazim Ali Al-Qureshi, Ph.D.
Coorientador: Prof. Dachamir Hotza, Dr.-Ing.

Florianópolis
2012

Catalogação na fonte elaborada pela biblioteca da Universidade Federal de Santa Catarina

A ficha catalográfica é confeccionada pela Biblioteca Central.

Tamanho: 7cm x 12cm

Fonte: Times New Roman 9.5

Maiores Informações em

http://www.bu.ufsc.br/design/Catalogacao.html

Leandro Neckel

MODELAMENTO E SIMULAÇÃO DE IMPACTO BALÍSTICO EM SISTEMA CERÂMICA-METAL

Esta Dissertação foi julgada adequada para obtenção do Título de Mestre em Ciência e Engenharia de Materiais, e aprovada em sua forma final pelo Programa de Pós Graduação em Ciência e Engenharia de Materiais.

Florianópolis, 9 de Março de 2012

_____

Prof. Carlos Augusto Silva de Oliveira, Dr.

Coordenador do Curso

Banca Examinadora:

_____	_____
Prof. Hazim Ali Al-Qureshi, Ph.D, Orientador, Presidente UFSC – CEM/EMC	Prof. Dachamir Hotza, Dr. Ing, Coorientador UFSC – EQA
_____	_____
Prof. Oscar Rubem Klegues Montedo, Dr. Eng, Membro Externo, UNESC	Prof. Márcio Celso Fredel, Dr. Ing, UFSC – EMC, Membro, UFSC
_____	
Prof. Carlos Pérez Bergmann, Dr. Ing, Membro Externo, UFRGS – DEM	

ACKNOWLEDGMENTS

Initially I would like to thank my master and advisor Prof. Hazim Ali Al-Qureshi, who made me “think like an engineer”, what is really hard for a person who holds a degree in Physics.

To the Universidade Federal de Santa Catarina and the Graduate Program of Materials Science and Engineering coordinators, professors and workers.

To my co-advisor, Prof. Dachamir Hotza, for the project support, as well as for the opportunity to spend a year in Hamburg.

To Dr. Rolf Janssen, my supervisor during my stay in Hamburg, for supporting my work in Hamburg.

To Dr. Acires Dias for the support to the Fracture and Damage Mechanics Conference in Croatia.

To the staff and fellow students during my time at TUHH: Manfred, Paula, Rodrigo, Hüssein, Wolfgang, Nils, Ezgi and Tobias. A special thanks for Anja, Bastian and Sascha, who helped me with every difficulty.

To my colleagues Murilo and João Gustavo for helping me with some engineering topics.

To my friends Alexandre, Adroaldo, Luis Paulo, Leonan and Mauricio who always pushed me forward when I was thinking of going back.

To my fiancée Camila with great affection who always encouraged me to never give up with her love and patience.

And to my family, for all the education, love and, specially, the insistence, because without you I would not be here.

Medicine makes people ill, mathematics make them sad and theology makes them sinful.

(Martin Luther)

ABSTRACT

New ballistic protection systems have been created recently based on high-tech materials. One of the industry's objectives is to develop lighter and stronger defensive systems, which allow higher mobility and greater safety for both vehicles and humans. This work studies mathematically the behavior of a protection against a projectile impact. The employed model, originally proposed by Al-Qureshi et al [1], includes a ceramic and metal layer system protection, and describes the projectile behavior and the impact absorption properties of the system. The literature also shows that the erosion tax and deceleration are highly dependent on the geometrical and structure parameters of the protective material. The phenomenon is described in different steps, presenting particular features for each step. The behavior equations present different system properties along the stages. This work presents a mathematical simulation performed on a developed model searching for best values for further studies. The properties to optimize include thicknesses of used plates, deforming profile, ceramic density, in addition to other relevant parameters. The program allowed the simulation of different parameters in the differential equations. As a result, graphs and surface plots were generated, which allowed a deeper analysis of the model and built an improved understanding of the process of fracture in materials by high velocity impact. Future studies will use these results as the basis for the manufacturing of a protection, which will be used for a practical experiment.

RESUMO

Novos sistemas de proteção balística vêm sendo recentemente criados com base em materiais de alta tecnologia. Um dos objetivos da indústria do ramo é desenvolver sistemas defensivos mais leves, porém mais fortes, que possibilitem ao portador, veicular ou humano, uma maior mobilidade com um maior nível de segurança. Este trabalho, baseado no trabalho original de Al-Qureshi et al [1], estuda matematicamente o comportamento de uma proteção contra um impacto de projétil. O modelo empregado inclui um sistema de proteção em camadas de cerâmica e metal, e ainda descreve o comportamento do projétil e as propriedades de absorção de impacto do sistema. A literatura ainda mostra que a taxa de erosão e desaceleração do projétil são altamente dependentes dos parâmetros geométricos e estruturais do material da proteção. O fenômeno de impacto e penetração é descrito em diferentes estágios, apresentando características particulares entre tais. As equações apresentadas demonstram diferentes propriedades do sistema ao longo dos estágios. Este trabalho ainda apresenta uma simulação matemática realizada sobre o modelo desenvolvido e aprimorado em busca de propriedades otimizadas do material para estudos futuros. Dentre as propriedades investigadas citam-se a espessura das placas utilizadas, o perfil de deformação do material metálico, a densidade da cerâmica, dentre outras características relevantes para o fenômeno. A rotina computacional possibilitou a aplicação de diferentes parâmetros nas equações propostas. Como resultado, gráficos e superfícies foram geradas, o

que possibilitou uma análise mais profunda do modelo e um maior entendimento do processo de fratura em materiais por impacto de alta velocidade. Estudos futuros utilizarão estes resultados e desenvolvimentos para a produção de uma proteção balística que será utilizada para um experimento prático.

FIGURE INDEX

TABLE INDEX

SYMBOL LIST

A Metal hardening law constant

A_p Projectile effective area

c Longitudinal velocity of the sound

d Radius of the projectile

dV Volume infinitesimal element

E Elastic modulus

E_c Elastic modulus of the ceramic material

E_k Kinetic energy of the projectile

E_m Elastic modulus of the metallic material

E_p Plastic energy absorbed by the metallic plate

e_c Thickness of the ceramic layer

e_m Thickness of the metallic Plate

HV Vicker's Hardness

h Thickness of the metal plate

k Deflection profile constant

k_{mod} Modified deflection profile constant

$m(t)$ Projectile mass function

m_{pr} Remaining mass of the projectile after the second stage

n Hardening index

R_c Resistance against ceramic penetration

r Radial distance

t Time

t_{fs} Duration of the first stage

$u(t)$ Interface velocity function

$v(t)$ Projectile velocity function

v_{pr} Projectile velocity in the end of the second stage

$w(r)$ Metal deflection profile function

w_0 Maximum deflection

Y_p Dynamic yielding of the projectile material

Greek letters

$\bar{\varepsilon}$ Average strain

ε_r Radial strain

ρ Density

ρ_c Density of the ceramic material

ρ_m Density of the metallic material

ρ_p Density of the projectile material

$\bar{\sigma}$ Average stress

TABLE OF CONTENTS

1 INTRODUCTION

1.1 Motivation

Ballistic protections are structures that have been much studied by different areas of science and engineering. Those materials are often applied in the transport, security and construction sectors. The impact energy absorption and its effects are decisive on the issue of security and reliability to its application. In this way, better protection against impacts is a milestone for the development of new mobility systems. As the research in materials advances, faster and safer protective systems for vehicles and/or buildings can be built.

Al-Qureshi et al.[1] have developed a mathematical approach to the high speed impact against a particular type of protection and have performed some experiments with the proposed geometry as well. The armor cited is a two-layer system of ceramic and metal. The ceramic is responsible for the erosion of the incident projectile, which reduces its kinetic energy. The function of the metal layer is to prevent the projectile of going through the shield by absorbing its final kinetic energy as a plastic deformation.

It is important to cite that the high speed impacts are phenomena presenting high complexity and limited reproduction. Parameters such as pressure, energy and projectile incidence in the protection, for example, can hardly be adjusted and/or prevented. In the literature [2,3,4,5] there are several high

complexity models using different methods. Modern mathematical approaches, such the work of Iqbal et al. [2] and Vanichayangkuranont et al. [5], present the interpretation of the impact phenomenon based on finite element modeling. On the other hand, further models based on simpler approaches with different objectives have been developed. The work of Jerz et al. [3] and Naik et al. [4] present approaches based on the projectile energy and the plastic and elastic deformation theory.

However, the focus of the presented model is to represent the proposed impact situation using a simple approximation by ordinary differential equations.

1.2 Objectives

This work has the main objective of understanding the impact phenomenon on the proposed structure with its effects in both projectile and protection.

To achieve this goal, the following objectives were set

- Solving the movement equations of the proposed model using numerical methods;
- Generating a routine to solve the same problem with different parameters of both projectile and protection;
- Improving the model by modifying the proposed equations in their deficiencies;
- Simulating the impact over the proposed structures with different types of projectiles.

2 LITERATURE REVIEW

2.1 Protection Modeling

The process of impact is described by Al-Qureshi et al. [1] in three different stages, showing different behavior of the projectile and the protection for each one. The first one explains the initial impact, analyzing the erosion of the head of the projectile and the loss of velocity without effective penetration. The second stage shows the behavior of the ceramic in the energy absorption during the penetration. In this stage, a movement of an interface projectile-ceramic as one factor of deceleration is considered. The third step of the phenomenon reports the absorption of the remaining energy of the projectile. For the three stages there are equations representing the evolution of the velocity and mass of the projectile. Moreover, for the third stage it is presented a deterministic equation for the maximum deformation of the metal plate.

2.2 The Geometry of the Protection

Generally, impact problems were primarily of concern to the military, either for defensive or offensive purposes to develop armor or ammunition[1]. High speed impacts must be considered in many other situations. For all of them, it is important to prevent the complete failure of the protection by improving the mechanical properties of the used materials. Impacts of this nature are studied by many authors and each one researches the most

efficient protection for a specific projectile. For this particular geometry, the impact of a metallic projectile, more specifically a bullet, is considered.

Basically, the protection is a double layer system made of ceramic and metallic plates as shown in Figure 2.1. The ceramic layer cited in the literature is made of alumina and has a thickness between 8 and 12 mm. This plate is the one that will support the initial impact. The secondary layer is made of metallic material. The original work[1] proposes using stainless steel 304 with 10 mm thickness. This layer also may have a larger area than the ceramic plate. In fact, this is not necessary, but helpful in the construction of the protection. In addition, a layer of aramide ply lined with sikaflex 221 resin was applied over the ceramic plate in order to retain the projectile fragments after each test [1] This also helps to glue both layers.

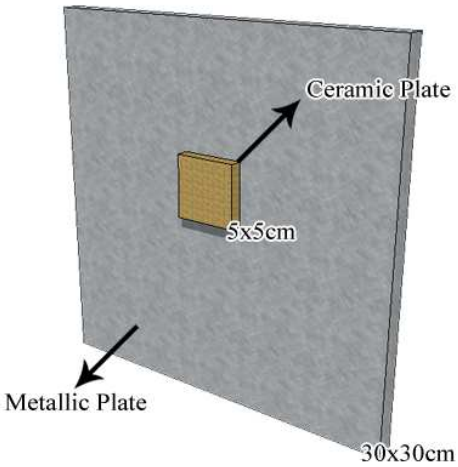

Figure 2.1: Proposal of a two layer protection made by Al-Qureshi et al. [1]

2.3 The Stages of Penetration

The penetration process is divided in three stages which represent the behavior of both projectile and protection during the impact and penetration processes. These differences have to be considered to understand the system after the high speed impact.

The first stage is related to the initial impact of the projectile in the ceramic. The impact generates a shock wave that travels through the shield and reflects back at the end of the protection. The generated wave is shown in Figure 2.2. The overlap of the incoming and reflected waves will crack the ceramic. This crack has a format of a cone due the wave overlapping process.

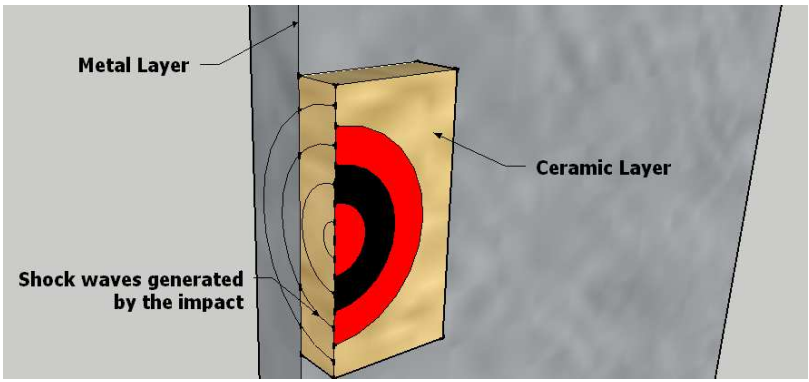

Figure 2.2: First stage of the impact. The collision generates a shock wave that travels through the armor.

An important factor that contributes in the first and second stage is the effect of the ceramic against the projectile. As known, the ceramic is brittle, but this material is incompressible after some pressure, which is very different from a metal. Once the projectile is made of metallic material, it is possible to prevent its

erosion in the high speed impact against the ceramic. In this case, the material of the first layer can be compared with powerful cutting tools with efficient machining capacity for the projectile material [6]. While the shock waves travel, the head of the projectile is eroded, but no effective penetration occurs.

The first stage ends when the wave returns to the generation point. Then, the wave overlapping ends and the ceramic is enough cracked to allow the projectile to penetrate effectively the first layer.

The second stage starts at same time. The process of effective penetration is analyzed in this stage. The projectile starts pushing an interface projectile-ceramic inwards the armor. This interface is responsible for the erosion in the projectile in this stage. It is important to observe that if there is no difference between the velocities of both projectile and interface, there will be no erosion. To better understand the process, it is necessary to consider the Tate's law for solids subjected to extremely high pressures [7]. According to it, it is assumed that the rod (projectile) act as rigid body until a certain pressure is reached, which is a constant for a given material. At pressures above this value the material behaves hydrodynamically. A similar argument may be applied to the target material. In this case, however, the pressure required to make material flow hydrodynamically must overcome not only the rigidity of the material in the immediate neighborhood but also the inertia of surrounding material. In this way, Tate introduces the modified hydrodynamic law for solids,

which is necessary for the comprehension of penetration phenomenon.

This stage lasts until the velocities of the projectile and interface are equal. When this occurs, the erosion stops and the rest of the projectile keep penetrating and deforming the metal plate, which represents the final stage. The transition between the second and third stage is not exactly when the metal plate starts deforming, because it happens almost in the end of the intermediate stage. In addition, the deflection of the plate is studied with deterministic equations, while the velocity of the projectile is analyzed using a kinetic approach.

The third stage is the final deceleration of the projectile. In this situation, the interface projectile-ceramic has the same velocity of the bullet and both decelerations are equal. The metal layer of the protection deforms plastically absorbing the remaining energy of the bullet. Moreover, the protection will not fail completely if the ceramic has absorbed enough energy before the deflection starts.

2.4 Equations of Movement

As the penetration process, the equations are also divided by stages. Basically there are equations for the erosion and deceleration of the projectile for all the stages except the third where there is no erosion of the bullet.

To erode the head of the projectile then the dynamic yielding (Y_p) of the projectile must be exceeded [1]. Then, the force opposing the penetration can be given as

$$m(t)\frac{d}{dt}v(t) = -Y_p A_p \tag{2.1}$$

This Y_p is one of the Tate's [7] constants and represents the maximum pressure that a solid supports before start behaving hydrodynamically. According to Tabor [8], the dynamic hardness of a metal is the pressure with which it resists local indentation by a rapidly moving indenter. The actual value of the dynamical yield pressure depends on the velocity of impact and on the way it is computed.

A_p is the projectile's head area. *m(t)* and *v(t)* are the function for mass and velocity of the projectile respectively. It is important to mention that mass is a function of time due the erosion of the bullet material. The erosion rate of the projectile is given by

$$\frac{d}{dt}m(t) = -\rho_p A_p v(t) \tag{2.2}$$

where ρ_p is the density of the projectile material.

In this stage there is no movement of interface and the head of the bullet is being eroded without effective penetration. The shock wave generated by the impact travels through the protection and reflects back returning to the collision point. The respective necessary time was calculated by Wilkins [9,10] and it is given by

$$t_{fs} = \frac{6e_c}{c} \tag{2.3}$$

where e_c is the thickness of the plate and *c* the longitudinal velocity of sound in the material.

When this time is reached, the rigidity of the material neighbor to the collision point is overcome and the bullet starts advancing through the ceramic. In this way, the movement of the interface projectile-ceramic begins. This fraction of the ceramic plate moves with velocity *u(t)* and is responsible for the erosion of the projectile during the second stage. In addition, in this intermediate stage, the force opposing the penetration remains the same.

The erosion rate in the second stage is given by

$$\frac{d}{dt}m(t) = -\rho_p A_p \left(v(t) - u(t)\right) \tag{2.4}$$

The configuration of the process during this stage can expressed by Tate's hydrodynamic modified law [8]

$$Y_p + \frac{1}{2}\rho_p \left(v(t) - u(t)\right)^2 = R_c + \frac{1}{2}\rho_c \left(u(t)\right)^2 \tag{2.5}$$

where R_c is the dynamic resistance strength against penetration into the ceramic [11], considered to be constant. This is the property related to the rigidity of the target proposed by Tate [7].

Simultaneously to the penetration of the projectile, the metallic base will move and will be deformed elastically. However, the energy produced by this elastic energy will be low and will be neglected [1]. The deformation of the metallic plate will be discussed in the next chapter.

As given by Eq. (2.4), the erosion will cease when both interface and projectile velocities are equal. Then, the second stage ends. After this occurs the projectile will continue penetrating the armor with deceleration given by

$$m_{pr}\frac{d}{dt}v(t) = -R_c A_p \tag{2.6}$$

Here, m_{pr} is the remaining mass of the projectile and due the absence of erosion, and it is not a function of time anymore.

2.5 Equations for the Metallic Plate Deformation

Due the deceleration of the bullet caused by the ceramic layer, the metallic plate may not be perforated. In this case, the secondary layer will suffer plastic deformation and the plastic energy consumed by the plate can be expressed in terms of effective stress and strain as

$$E_p = \int_v \left(\int_0^{\bar{\varepsilon}} \bar{\sigma} \partial \bar{\varepsilon} \right) dV \tag{2.7}$$

For a material with effective stress–strain curve of a power-law hardening expression

$$\bar{\sigma} = A\left(\bar{\varepsilon}\right)^n \tag{2.8}$$

Then, the total plastic energy becomes

$$E_p = \frac{A}{n+1}\int_v \left(\bar{\varepsilon}\right)^{n+1} dV \tag{2.9.}$$

Assuming that the material will be bulged in an axis symmetric mode, the effective strain can be written in terms of the radial strain as

$$\bar{\varepsilon} = 2\varepsilon_r \tag{2.10}$$

For a small displacement, the radial strain can be approximated to [1,12,13]

$$\varepsilon_r = \frac{1}{2}\left(\frac{\partial}{\partial r} w(r)\right)^2 \qquad 2.11$$

where the function *w(r)* is the deflection profile of the impact. Thus

$$\bar{\varepsilon} = \left(\frac{\partial}{\partial r} w(r)\right)^2 . \qquad 2.12$$

The geometry of the small dimple done by the impact can be approximated as a small cylinder. The element of volume can be expressed as

$$dV = 2\pi r h \partial r \qquad 2.13$$

where *h* is the thickness of the plate. The substitution of Eqs. (2.12) and (2.13) into Eq. (2.9) gives

$$E_p = \frac{2\pi h A}{n+1}\int_0^{\infty}\left(\frac{\partial}{\partial r} w(r)\right)^{2(n+1)} r\partial r . \qquad 2.14$$

For the solution of Eq. (2.14) is necessary to determine the deflection profile. Al-Qureshi et al. [14] have found that this profile can be expressed by an exponential given as

$$w(r) = w_0 e^{\left(-\frac{k}{d}r\right)} \qquad 2.15$$

where w_0 is the maximum deflection of the dimple at $r = 0$, and *k* is the deflection profile that can be determinate experimentally or by numerical adjustment. Moreover, it is necessary to consider the effect of the projectile geometry in the profile. Then, the constant *d*, which represents the bullet radius, was included in the equation. The differentiation of Eq. (2.15) gives

$$\frac{\partial}{\partial r} w(r) = w_0 \left(-\frac{k}{d} \right) e^{\left(-\frac{k}{d} r \right)} \quad . \qquad 2.16$$

that furnishes the deflection profile necessary in the Eq. (2.14).

Substituting Eq. (2.16) into Eq. (2.14) gives

$$E_p = \frac{2\pi h A}{n+1} \left(-\frac{k w_0}{d} \right)^{2(n+1)} \int_0^{\infty} e^{\left[\frac{-kr(2n+2)}{d} \right]} r \partial r \quad . \qquad 2.17$$

It is known that the strain hardening index *n* is fractional (*0 < n < 1*) and this will generate a complex value as result of $\left(-\frac{k w_0}{d} \right)^{2(n+1)}$.

Considering the physical nature of most constants it is possible to suppress the negative sign generated by the derivation demonstrated in Eq. (2.17). Also, the radial variation of the deflection profile is mirrored in the x-axis, which demonstrates that this ratio can be used as its own module. Now it gives

$$E_p = \frac{2\pi h A}{n+1} \left(\frac{k w_0}{d} \right)^{2(n+1)} \int_0^{\infty} e^{\left[\frac{-kr(2n+2)}{d} \right]} r \partial r \quad . \qquad 2.18$$

The solution for the expression is given by

$$E_p = \frac{1}{2} \frac{\pi h A \left(\frac{k}{d} \right)^{2n} w_0^{2(n+1)}}{(n+1)^3} \qquad 2.19$$

that can be written as

$$E_p = B\left(w_0^{2(n+1)} \right) \qquad 2.20$$

where

$$B = \frac{1}{2}\frac{\pi h A}{(n+1)^3}\left(\frac{k}{d}\right)^{2n} \quad . \tag{2.21}$$

According to Al-Qureshi et al. [1], a close examination of Eq. (2.16), reveals that the absorbed energy is directly proportional to the plate thickness, and is greatly influenced by the work hardening characteristics of the material.

After the initial impact, the movement of the interface starts deforming the metallic plate. It can be argued that, initially, the metal layer is compressed due to high pressure generated by the impact. In addition, the plate does not move significantly because of the low interface velocity. In this way, it is possible to affirm that the deflection of stainless steel plate starts at the end of the second stage of penetration.

Considering this, the energy absorbed by the plate can be approximately equated to the kinetic energy at the end of the second stage, which gives

$$E_k = \frac{1}{2} m_{pr} v_{pr}^2 = E_p \tag{2.22}$$

where v_{pr} is the velocity of the projectile in the end of the second stage. It gives

$$\frac{1}{2} m_{pr} v_{pr}^2 = B\left(w_0^{2(n+1)}\right) \tag{2.23}$$

and, then, the maximum deflection of the plate can be written as

$$w_0 = \left(\frac{1}{2} \frac{m_{pr} v_{pr}^2}{B} \right)^{\frac{1}{2(n+1)}} \quad . \qquad 2.24$$

2.6 Initial Results

Al-Qureshi et al. [1] have performed some experiments based on the presented model. The target was attached to a special fixture to ensure a normal impact condition. Moreover, the experimental apparatus allowed measuring the initial velocity of the projectile in the collision. After each test, the maximum central deformation of the base (w_0) and the residual mass of the projectile (m_{pr}) were measured. These tests permitted to compare the theoretical and the experimental data. Then, these variables were used to determine the influence of the grain size on the efficiency of the shield.

The projectile properties are shown in Table 2.1. The same projectile caliber was used for all the experimental tests. The ceramic presented a thickness of 7.3, 9.3 and 11.3 mm. The ceramic plates were manufactured from the same chemical composition, but having different grain sizes. They were obtained by mixing different proportions of calcinated alumina A-1000SG and tubular alumina T-60 (both provided by Alcoa), and 2% TiO_2 was added for the sintering operation. Table 2.2 lists the formulations used for those experiments [1].

The mechanical properties of the different ceramic compositions are listed in Table 2.3.

Table 2.1: Projectile properties.

Property	Steel Nucleus of the Projectile
Initial Velocity (*m/s*)	835
Mass (*g*)	9.54
Vicker's Hardness (*HV*)	817.5
Dynamic Yield Stress (*GPa*)	2.82
Density (g/cm^3)	8.41
Diameter (*mm*)	7.62

Table 2.2: Ceramic compositions.

Composition	Al_2O_3 A-1000SG (wt.%)	Al_2O_3 Tubular T-60 (wt.%)	TiO_2 (wt.%)
A	95	3	2
B	90	8	2
C	85	13	2
D	80	18	2

In addition, the stainless steel 304 had the following hardening power law

$$\overline{\sigma} = 935\left(\overline{\varepsilon}\right)^{0.29} \quad MPa \tag{2.25}$$

and density of 7.77 g/cm^3.

For comparison, the maximum deflection of the metal plate was calculated theoretically for all the different thicknesses of the ceramic plate. The examination of this values shows that the values predicted by the theory are generally in good agreement with experimental results. The difference between experimental and theoretical data can be attributed to several factors such as the fact that the projectile does not collide perpendicularly to the target. Also, the variation in the thickness of the ceramic and the density may affect the results. Other important factor is that the theory considers that the transverse sectional area of the projectile (A_p) remains constant during the impact. This area is calculated based on the caliber of the projectile and then the theoretical fraction of mass lost in the impact was expected to be different of the experimental data. This comparison is shown in Table 2.4.

Table 2.3: Summary of mechanical and physical properties of various compositions

Property Composition	A	B	C	D
Modulus of Weibull (m)	14.4	8.4	8.8	15.1
σ50 (MPa)	203.7	175.0	171.3	161.3
σ0 (MPa)	209.0	182.8	178.5	165.2
Vicker's Hardness (HV)	-	1551.4	1259.8	-
Rc (GPa)	-	4.43	3.60	-
Density (g/cm^3)	3.79	3.90	3.80	3.75
Average Grain Size (μm)	-	18±8	22±9	-

V_{50} is defined as the limit impact velocity for the protection. It represents the velocity that causes partial or total penetration. From this investigation, it was found that the ceramic with composition C has an average V_{50} higher than the plate with composition B. This evidence indicates that the grain size has an important influence on the absorber energy. Needless to say, more experimental results are needed before any final conclusion can be drawn with respect to the influence of grain size on the absorbing energy behavior [1]. Thus, it is important to consider that is necessary to have more experimental data before any final conclusion about the grain effect in the efficiency of the shield.

The analytical result for the evolution of both of the projectile and the interface velocities is shown in Figure 2.3. In this Figure, the projectile velocity *v(t)* is written as $V_p(t)$ and the interface velocity *u(t)* as $V_i(t)$. The final deceleration (the third stage) of the projectile is not demonstrated in this Figure. In this case, it is possible to observe that the interface velocity was zero during the first stage. On the other hand, the interface starts moving in the second stage until it reaches the same speed as the projectile. After this, as already mentioned, the erosion ceases and both the projectile and the interface move together with same velocity.

Table 2.4: Comparison between theoretical and experimental values

Thickness of ceramic, e_c (mm)	**Composition**	**Impact Velocity, V_p (m/s)**	**Maximum Deflection, w_0 (mm)**		
			Exp.	Theory	Error (%)
11.3	B	792.7	16.5	17.0	-2.9
11.3	C	858.2	20.0	17.6	+13.6
9.3	B	628.9	18.0	17.8	+1.1
9.3	C	651.1	17.5	17.7	-1.1
7.3	B	428.8	15.5	17.3	-10.4
7.3	C	448.4	13.0	16.6	-21.7

The graph also shows that the second stage lasts more than the others revealing the importance of the ceramic layer in the energy absorption. In this case, it is possible to presume that different thicknesses of the ceramic layer will change the behavior of the shield in the impact situation. The use of thicker ceramic plates will increase the structure weight considerably and will reduce the deformation of the metal plate. On the other hand, ceramic with low thickness may not absorb enough energy of the projectile, which can cause total fracture of the armor.

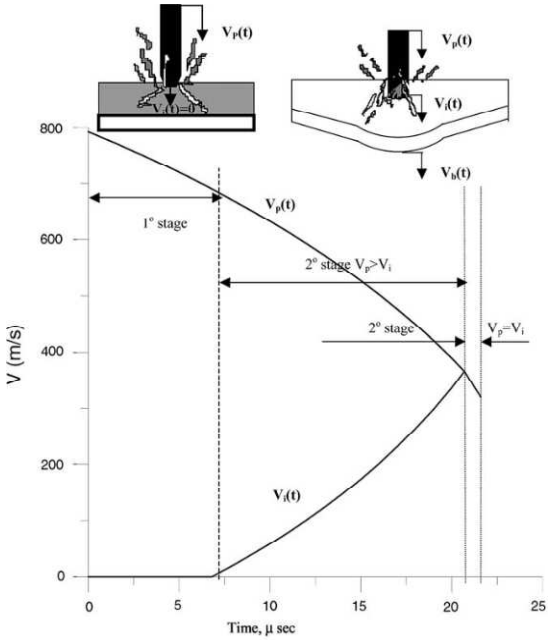

Figure 2.3: Projectile velocity as a function of penetration time.

3 SOLVING THE MODEL

Considering the present mathematical model, it is necessary to solve the equations to completely understand the behavior of the projectile and target in the situation of impact. Basically two different solutions can be found from the equations: one for the evolution of the mass and another for the velocity during the collision. Then, the solution for the interface velocity can be found from the kinematic equations system. On the other hand, the maximum deformation of the metallic plate after the impact can be calculated by using the deterministic equations of absorbed energy.

The division of the mathematical model in stages makes impossible to find a unique solution for the velocity or for the mass for the entire phenomenon. Considering this, the search for the solution of the impact evolution is also divided in stages, but then, all data are merged and a unique curve can be plotted. Then, for a more convenient and organized solution, the solutions are separated into mass and velocity equations for each stage, which makes necessary the manipulation and separation of the differential equations in a characteristic mathematical sentence for each situation.

After finding the equations of mass and velocity for each stage, it is possible to solve them by using numerical methods. In this way, initial conditions and constants values are required and can be easily found in the original work. At the shift of the first to the second stage the conditions of continuity are applied for both

mass and velocity. At the shift for the third stage, the continuity condition for the velocity is once more applied, but not for the mass since it is constant in this stage.

Since the kinematic equations are solved and the solutions are merged, it is possible to predict how much the metal plate will be deformed by applying values in the deterministic equation of deflection. The resulting values can be compared with some few results found in the original work. Moreover, the numeric values necessary for the constants involved in this equation can be found in Al-Qureshi's work [1].

In the next chapters, the general method presented above will be explained in detail.

3.1 Equation for the Projectile Velocity in the First Stage

For the three stages, it is necessary to manipulate the equations to find a unique differential equation for the function of the mass and the velocity of the projectile. Needless to say, the function for the mass does not have to be solved for the third stage because it is constant.

The differential equation for the velocity on the first stage can be found firstly considering both equations of the model for the first stage. The force against the projectile is given by

$$m(t)\frac{d}{dt}v(t) = -Y_p A_p \qquad 2.1$$

and the erosion tax is given by

$$\frac{d}{dt}m(t) = -\rho_p A_p v(t) \qquad 2.2$$

.

First, the equation (2.1) can be derived in function of time giving

$$\left(\frac{d}{dt}m(t)\right)\left(\frac{d}{dt}v(t)\right)+m(t)\left(\frac{d^2}{dt^2}v(t)\right)=0 \quad . \qquad 3.1$$

Now it is possible to substitute the erosion tax given by (2.2) in the equation (3.1). It gives

$$-\rho_p A_p v(t)\left(\frac{d}{dt}v(t)\right)+m(t)\left(\frac{d^2}{dt^2}v(t)\right)=0 \quad . \qquad 3.2$$

Also, it is possible to isolate the function *m(t)* in the equation (2.1), which is necessary for the equation (3.2). It gives

$$m(t)=-\frac{Y_p A_p}{\left(\frac{d}{dt}v(t)\right)} \qquad 3.3$$

Substituting equation (3.3) into (3.2) gives

$$-\rho_p A_p v(t)\left(\frac{d}{dt}v(t)\right)-\frac{Y_p A_p\left(\frac{d^2}{dt^2}v(t)\right)}{\left(\frac{d}{dt}v(t)\right)}=0 \qquad 3.4$$

that can be simplified and written as

$$\frac{d^2}{dt^2}v(t)=-\frac{\rho_p v(t)\left(\frac{d}{dt}v(t)\right)^2}{Y_p} \qquad 3.5$$

The differential equation given by the expression (3.5) can be solved using numerical methods. The computational structure of the solving method will be explained in the next chapters.

It is interesting to mention that the velocity does not depend on the effective area of the projectile. On the other hand, it was expected that the higher the dynamic yielding Y_p of the projectile material, the lower the deceleration.

3.2 Equation for the Projectile Mass in the First Stage

To find the differential equation for the mass of the projectile in the first stage, it is again necessary to manipulate the expressions in function of the time for the first stage given by the equation (2.1) and (2.2). The derivation of equation (2.2) gives

$$\frac{d^2}{dt^2} m(t) = -\rho_p \, A_p \left(\frac{d}{dt} v(t) \right) \tag{3.6}$$

By isolating the acceleration term in the equation (2.1) it gives

$$\frac{d}{dt} v(t) = -\frac{Y_p \, A_p}{m(t)} \tag{3.7}$$

and this expression can substituted in the equation (3.6). Then the expression for the mass of the projectile in the first stage can be written as

$$\frac{d^2}{dt^2} m(t) = \frac{\rho_p A_p^2 Y_p}{m(t)} \tag{3.8}$$

Here the importance of the geometry of the material can be noticed. The effective area, which is calculated using the diameter of the projectile, has a very high influence in the erosion tax. It is possible to note that the erosion tax will become lower

with the time. This can be explained by the drastic decrease of kinetic energy due to reduction of speed and mass.

In addition, it is known that the variation of the mass during the impact implies a variation in the projectile geometry. However, in this work the projectile area (A_p) during the whole phenomenon is considered constant.

3.3 Equation for the Projectile Velocity in the Second Stage

The second stage starts when the wave generated by the impact reflects back in the end of the protection and returns to the original point. After this, the movement starts being governed by different equations due to the existence of the interface projectile-ceramic movement. Again, to find the characteristic differential equation for the velocity in the second stage of penetration it is necessary to manipulate the equations given by Al-Qureshi's model.

The force against the projectile remains the same as the first stage and it is given by

$$m(t)\frac{d}{dt}v(t) = -Y_p\, A_p \qquad 2.1$$

and the erosion tax is now given by

$$\frac{d}{dt}m(t) = -\rho_p\, A_p \left(v(t) - u(t)\right) \qquad 2.4$$

where *u(t)* represents the interface velocity.

Then, for dealing with the problem of the velocity and mass for the second stage, it is necessary to use the Tate's hydrodynamic modified law for solids given by

$$Y_p + \frac{1}{2}\rho_p \left(v(t) - u(t)\right)^2 = R_c + \frac{1}{2}\rho_c \left(u(t)\right)^2 \qquad 2.5$$

where R_c is the resistance of the ceramic against the penetration and ρ_c is the ceramic density.

From the equation (2.4) is possible to obtain

$$u(t) = \frac{\frac{d}{dt}m(t)}{A_p \rho_p} + v(t) \qquad 3.9$$

and from equation (3.1), which is also valid for the second stage, is possible to isolate the erosion tax, which gives

$$\frac{d}{dt}m(t) = -\frac{m(t)\left(\frac{d^2}{dt^2}v(t)\right)}{\left(\frac{d}{dt}v(t)\right)} \qquad 3.10$$

The replacement of equation (3.10) into (3.9) gives

$$u(t) = -\frac{m(t)\left(\frac{d^2}{dt^2}v(t)\right)}{\left(\frac{d}{dt}v(t)\right)A_p \rho_p} + v(t) \qquad 3.11$$

and can be simplified using equation (3.3), which gives

$$u(t) = \frac{Y_p\left(\frac{d^2}{dt^2}v(t)\right)}{\left(\frac{d}{dt}v(t)\right)^2 \rho_p} + v(t) \qquad 3.12$$

Tate's equation (2.5) presents only the functions for the projectile and interface velocities and also can be manipulated to be written as a second degree equation for the function *u(t)*:

$$u(t)^2\left(\rho_c-\rho_p\right)+2\rho_p\, v(t)\,u(t)+2R_c-2Y_p-\rho_p\, v(t)^2=0 \qquad 3.13$$

where, in the $ax^2+bx+c=0$ format, the constants *a*, *b* and *c* are

$$a=\left(\rho_c-\rho_p\right)\quad;\quad b=2\rho_p\, v(t)\quad;\quad c=2R_c-2Y_p-\rho_p\, v(t)^2 \qquad 3.14$$

The solution for the equation (3.13) is given by

$$u(t)=\frac{\rho_p\, v(t)-\sqrt{\rho_c\,\rho_p\, v(t)^2-2\,\rho_c\,R_c+2\,\rho_c\,Y_p+2\,\rho_p\,R_c-2\,\rho_p\,Y_p}}{\rho_p-\rho_c} \qquad 3.15$$

Now, substituting equation (3.15) into (3.12) is obtained

$$\frac{Y_p\left(\frac{d^2}{dt^2}v(t)\right)}{\left(\frac{d}{dt}v(t)\right)^2\rho_p}+v(t)=\frac{\rho_p\, v(t)-\sqrt{\rho_c\,\rho_p\, v(t)^2-2\,\rho_c\,R_c+2\,\rho_c\,Y_p+2\,\rho_p\,R_c-2\,\rho_p\,Y_p}}{\rho_p-\rho_c} \qquad 3.16$$

that can be simplified finding the characteristic differential equation for the velocity on the second stage:

$$\frac{d^2}{dt^2}v(t)=\frac{\rho_p\left(\frac{d}{dt}v(t)\right)^2\left(\rho_p\, v(t)-\sqrt{\rho_c\,\rho_p\, v(t)^2-2\,\rho_c\,R_c+2\,\rho_c\,Y_p+2\,\rho_p\,R_c-2\,\rho_p\,Y_p}\right)}{Y_p\left(\rho_p-\rho_c\right)} \qquad 3.17$$

The positive signal in the solution of the second degree equation was suppressed due to the possible complex solutions. Since the phenomenon is purely physical and real, it makes

absolutely no sense to consider imaginary solutions for the problem.

3.4 Equation for the Projectile Mass in the Second Stage

The same manipulation has to be done to find the differential equation for the erosion of the projectile in the second stage. Initially, it is possible to substitute equation (3.9) into (3.15), which gives

$$\frac{\frac{d}{dt}m(t)}{A_p \rho_p} + v(t) = \frac{\rho_p v(t) - \sqrt{\rho_c \rho_p v(t)^2 - 2\rho_c R_c + 2\rho_c Y_p + 2\rho_p R_c - 2\rho_p Y_p}}{\rho_p - \rho_c} \quad 3.18$$

that needs to be manipulated by isolating the function of velocity, which gives

$$v(t) = \frac{-\rho_c\left(\frac{d}{dt}m(t)\right) + \sqrt{2\rho_c\rho_p^2 Y_p A_p^2 - 2\rho_c\rho_p^2 R_c A_p^2 + \rho_c\rho_p\left(\frac{d}{dt}m(t)\right)^2}}{\rho_c\rho_p A_p} \quad 3.19$$

This equation can be derived in function of *t* giving

$$\frac{d}{dt}v(t) = \frac{-\rho_c\left(\frac{d^2}{dt^2}m(t)\right) + \frac{\rho_c\rho_p\left(\frac{d}{dt}m(t)\right)\left(\frac{d^2}{dt^2}m(t)\right)}{\sqrt{2\rho_c\rho_p^2 Y_p A_p^2 - 2\rho_c\rho_p^2 R_c A_p^2 + \rho_c\rho_p\left(\frac{d}{dt}m(t)\right)^2}}}{\rho_c\rho_p A_p} \quad 3.20$$

Here it is possible to use the equation (3.7) once more. Then it gives

$$-\frac{Y_p A_p}{m(t)} = \frac{-\rho_c\left(\frac{d^2}{dt^2}m(t)\right) + \frac{\rho_c\rho_p\left(\frac{d}{dt}m(t)\right)\left(\frac{d^2}{dt^2}m(t)\right)}{\sqrt{2\rho_c\rho_p^2 Y_p A_p^2 - 2\rho_c\rho_p^2 R_c A_p^2 + \rho_c\rho_p\left(\frac{d}{dt}m(t)\right)^2}}}{\rho_c\rho_p A_p} \quad 3.21$$

that can be written with the second derivative of the mass function isolated, which gives

$$\frac{d^2}{dt^2}m(t) = -\frac{\rho_c\rho_p A_p^2 Y_p}{m(t)\left(-\rho_c + \frac{\rho_c\rho_p\left(\frac{d}{dt}m(t)\right)}{\sqrt{2\rho_c\rho_p^2 Y_p A_p^2 - 2\rho_c\rho_p^2 R_c A_p^2 + \rho_c\rho_p\left(\frac{d}{dt}m(t)\right)^2}}\right)} \quad 3.22$$

The expression above is the characteristic differential equation for the loss of the mass in the second stage of penetration. Needless to say, both mass and velocity evolutions in the intermediary stage are strongly influenced by the projectile and ceramic materials properties. Then, at the end of this stage a small compression in the metal layer is initiated. However, due to the high speed and kinetic energy of the projectile, the effect of the resistance to the plastic deformation of the stainless steel plate was neglected.

The second stage ends when the erosion ceases. In this situation both interface and projectile velocities are equal and the loss of mass flux becomes zero. This is easily observable in equation (2.4). Considering this, the constant mass can be represented as m_{pr} in the third stage equation given by

$$m_{pr}\frac{d}{dt}v(t) = -R_c A_p \qquad 2.6$$

that can be solved with simple analytical methods. However, respecting the chosen methodology, the numerical method was once more chosen to find the solution. The method will be demonstrated in the next chapters.

3.5 Duration of the First Stage

To start solving the differential equations of the first stage, it is necessary to know how much time this initial part of the phenomenon will last. Considering the equation (3), it is possible to calculate this time due to the geometric parameters of the protection. The time of the first stage is given by

$$t_{fs} = \frac{6e_c}{c} \qquad 2.3$$

where e_c is the thickness of the ceramic layer and c the longitudinal velocity of sound in the material. For plates having 10 mm thickness, the time to form the fracture cone is approximately equal to 6 μs [1], which was used for the initial calculations.

In the end of the first stage, it is necessary to apply continuity conditions to the problem. It means that the final values for mass and velocity and their rates must be equal at the end of the first stage and at the beginning of the second stage. The same occurs at the end of the second stage with the velocity. It is necessary to mention that the influence of the epoxy resin between the ceramic and metal layer was not considered in the solution since it was also not take in account in the original model.

The erosion rate in the third stage is zero and the continuity condition does not need to be applied in this case. Moreover, the numerical method for solution and the storage method for the numerical values of the solution allow the easier manipulation of the data. These methods will be explained in the next chapters.

3.6 Solving the Movement and Mass Problems

The software Maplesoft Maple V12 was used to solve the equations and also to manipulate the data generated by the process of numerical solution. Firstly it was necessary to declare the characteristic differential equations for mass and velocity for the first stage. Then, it was also necessary to input the initial conditions for the problem. The second degree ordinary differential equation need two initial conditions: the primary condition is a value of the function in a specific value of abscise, and the secondary condition is a value of the first derivative in the same value of abscise of the primary condition. Needless to say that was also necessary to declare the numerical value for all the constants in the equations.

All the required constants values can be found in Al-Qureshi's [1] work and are presented in Table 3.1.

Table 3.1: Values for the constants of the differential equation.

Constant	Value
Y_p	2.82 GPa
A_p	45.58 mm²
ρ_p	8.41 g/cm³
R_c	4.43 GPa
ρ_c	3.90 g/cm³

The dynamic yielding Y_p of the projectile material is considered constant during all collision. Moreover, the value of A_p was calculated using the diameter of the projectile (7.62 mm) and it was also considered constant during all impact. The values of R_c and ρ_c are from the composition B (90% Al_2O_3 A-1000SG , 8% Al_2O_2 tubular T-60 , 2% TiO_2) which had an average grain size of 18.4 μm.

The primary initial conditions for the ordinary differential equations can be also find in the original work and are shown in Table 3.2

Table 3.2: Basic initial parameters.

Input	Value
Initial velocity *: v(t=0)*	*835.0 m/s*
Initial mass *: m(t=0)*	*9.54 g*

Considering the second degree differential equations, it is also necessary to introduce the secondary initial conditions. Those conditions can be deduced from the original equations. Table 3.3 presents those conditions.

The process of computing also must be stopped at the correct time, otherwise the solution will be obtained for times longer than the duration of the first stage. For the same stage the software was programmed to generate sixty values for the evolutions of mass and velocity. With these values, it is already possible to plot the first stage curves of mass and velocity.

To the second stage, it is necessary to apply continuity conditions. The final values in the first stage have to be considered the initial parameters for the second stage equations. Then, considering the second order ordinary differential equations, it is necessary to input the final values of the derivative of mass and velocity in the first stage as initial parameters for the second stage too.

Table 3.3: Secondary initial conditions.

Input	***Value***
Initial acceleration $\frac{d}{dt}v(t=0) = -\frac{Y_p A_p}{v(t=0)}$	*-1.34*10^7 m/s²*
Initial mass rate $\frac{d}{dt}m(t=0) = -\rho_p A_p v(t=0)$	*-320.08 kg/s*

The values of mass and velocity in the end of the first stage can be picked from the numerical solutions. Otherwise, the values of the derivatives must be calculated using the main equations of the second stage of penetration. The equations are

$$\frac{d}{dt}v(t) = -\frac{Y_p A_p}{m(t)} \qquad 3.7$$

and

$$\frac{d}{dt}m(t) = -\rho_p A_p \left(v(t) - u(t)\right) \qquad 2.4$$

.

In the second stage the interface projectile-ceramic starts to move with velocity *u(t)*. This velocity is null in the beginning of this stage and can be considered this way in equation 2.4 to find the secondary initial parameters. The final results for mass and velocity in the first stage are demonstrated in Table 3.4 and the secondary initial parameters are shown in Table 3.5.

With the equations and initial conditions declared, it is now possible to program the software to solve the second stage equations. The stop criteria for the calculations must be the value of time when the velocity of projectile is the same as the speed of the interface projectile-ceramic. For this, it is necessary to compare both numerical solutions. Unfortunately, the solution for the interface velocity depends on the solutions for velocity and erosion rate, as shown in equation (3.9).

Table 3.4: Initial parameters for the second stage differential equations.

Input	Value
Velocity at the end of 1st stage ***v(t=6μs)***	*745.11 m/s*
Mass at the end of first stage ***m(t=6μs)***	*7.71 g*

Table 3.5: Secondary initial parameters for the second stage differential equations.

Input	Value
Acceleration: beginning of the 2nd stage $\frac{d}{dt}v(t=6\mu s) = -\frac{Y_p A_p}{v(t=6\mu s)}$	*-1.66*10^7 m/s²*
Erosion rate: beginning of the 2nd stage $\frac{d}{dt}m(t=6\mu s) = -\rho_p A_p\left(v(t=6\mu s) - \underbrace{u(t=6\mu s)}_{(=0\,m/s)}\right)$	*-285 kg/s*

This problem is solved by firstly guessing an exaggerated value for the duration of the second stage. Then the equations of velocity and mass are solved for this amount of time. After that, it is possible to apply those values into the equation (3.9) generating the solution for the interface. Comparing both velocity solutions, it is now possible to exclude the extrapolated data and

find the correct duration for the second stage. This can be done by comparing the plots of interface and bullet velocities or comparing the row of generated data for both solutions. Moreover, if the guessed time was not enough to find the value of *t* when *v(t)=u(t)*, it is still possible to change the guessed value and compute the solution once more.

Considering and applying the process mentioned above, the duration for the second stage was 17.6 μs, with overall time of 23.6 μs in the end of the same stage.

The data generated for mass and velocity of the projectile in the end of the second stage are the values that must be applied in the formula for deformation of the metallic plate. It is also important to remember that the model considers that before the third stage the metallic plate suffers only small elastic deformation and, taking this into account, such effect is neglected in the equations. Applying the data in the deflection equation will be presented in the next chapters.

The third stage problem for the velocity can be solved using analytical methods. However, the numerical method is once more selected to solve the differential equation. This choice allows the solution to be manipulated equally as the solutions for the first and second stages.

The differential equation for the third stage can be found from equation 2.6, that gives

$$\frac{d}{dt}v(t) = -\frac{R_c A_p}{m_{pr}} \qquad 3.23$$

with the primary initial condition

$$v_{pr} = v(t = 23.6\mu s) = 322.03\, m/s \tag{3.24}$$

Considering that the first order differential equations require just one initial condition, here it is not necessary to declare the secondary initial parameters. Then, the remaining mass of the projectile m_{pr} is obtained from second stage solutions. Its value is

$$m_{pr} = m(t = 23.6\mu s) = constant = 3.01g \tag{3.25}$$

The duration of the third stage can be deducted from the analytical solution of equation (3.23) that gives

$$t_{ts} = -\frac{v_{pr}\, m_{pr}}{R_c\, A_p} \tag{3.26}$$

where t_{ts} is the duration of the third stage and v_{ts} is the initial velocity of the third stage. Then, the complete numerical solution for the problem of mass and velocity during the impact is solved.

The numerical data generated by the program can be plotted in a graph of velocity against time presented by Figure 3.1.

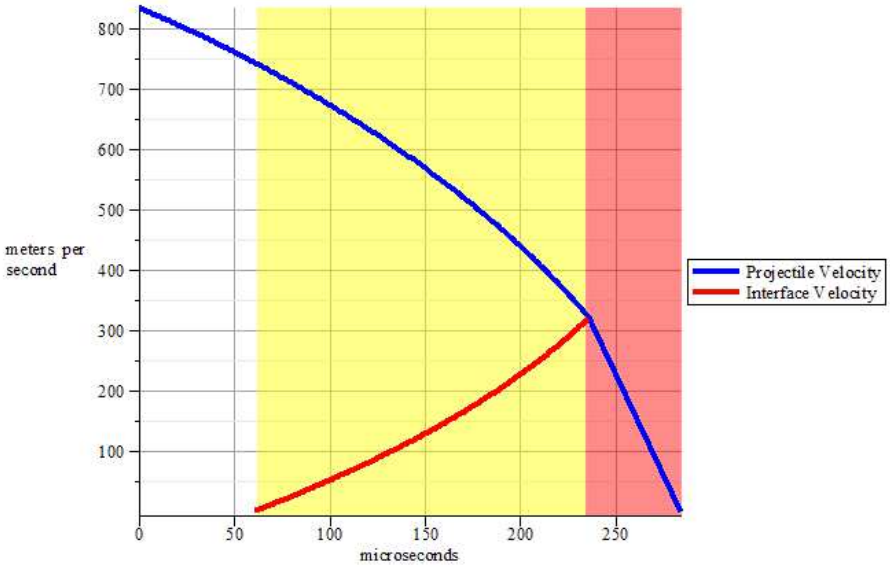

Figure 3.1: Evolution of the velocities of projectile and interface.

The regions in the plot show the different stages of penetration. The yellow region represents the second stage and starts with the interface velocity. The third region shows the third stage and starts when the speed of the projectile and interface are equal.

The blue line shows a shift in the curvature when the third stage begins. This can be explained due to the nature of the differential equations of velocity for each stage. Due to the independency of the own function, the solution of a first order differential equation is represented by a linear drawing.

The ceramic plate acts mainly in the first and second stages, when most of the kinetic energy is absorbed. The loss of velocity in the third stage can be associated principally to the

effect of the plastic deformation in the metallic plate. Table 3.6 shows the absorption of velocity, the loss of mass and the energy absorbed during the stages in percentages.

The results for the projectile velocity in the second stage, when the main penetration occurs, also permit the calculation of the depth reached by the projectile inside the ceramic tile. This can be easily performed by simple numerical integration of the values generated by the software. Using this technique with the generated values, the calculated depth is 9.8 mm.

Table 3.6: Deceleration, erosion and energy absorption rates among the stages.

Stage	Velocity Loss (%)	Erosion (%)	Absorbed Energy (%)
1°	*10.77*	*19,18*	*35.65*
2°	*50.67*	*49.27*	*59.66*
3°	*38.57*	-------	*4.69*

3.7 Calculating the Metallic Deformation

The main work made by Al-Qureshi et al. [1] also presents some experimental results. However, in the same work, there are only results for the final deformation w_0 of the metallic plate after the impact and no results for the remaining mass of projectile is furnished. Those experimental values were also compared with theoretical results calculated using the equation for the metallic plate deformation

$$w_0 = \left(\frac{1}{2} \frac{m_{pr} v_{pr}^2}{B} \right)^{\frac{1}{2(n+1)}} \qquad 2.24$$

where

$$B = \frac{1}{2} \frac{\pi h A}{(n+1)^3} \left(\frac{k}{d} \right)^{2n} \qquad .2.21$$

The final deformation of the metallic plate can also be calculated using the results of mass and velocity given by equations (3.24) and (3.25). Further constants involved in the

equation are also presented in the original work, except for the deflection profile *k* that, according to the author, can be determined experimentally [1]. Due to the necessity of this constant in the calculations, its value has to be calculated using the presented results with a regression procedure solving the equation 2.24 by isolating the value of *k.* Then, this parameter is considered as a property of the metallic material and also invariable. The value of other parameters present in the equations 2.24 and 2.21 are presented in Table (3.7):

Table 3.7: Values of the constants involved in equations 2.24 and 2.21.

Constant	Value
n	*0.29*
h	*1.5 cm*
A	*935 MPa*
d	*3.81 mm*
k	*0.0017*

With these values the result for the final deformation of the metallic plate is 16.2 mm, which is suitable to the theoretical results presented in the main work [1] according to Table 2.4.

4 MODIFYING THE MODEL

4.1 Duration of the First Stage

The original equation for the first stage duration was proposed by Wilkins [9,10] for a three layered ceramic structure. In the present work, the same approach was considered for the ceramic layer. However, it was necessary to improve the accuracy of the model and it was also possible to consider that the shock waves travel through all the structure. Thus, a modification in the proposed sentence for the duration of the first stage was done.

For a solid two layered system, it is necessary to consider the time needed for the generated wave to reflect in the back part of the protection and return to the initial point and, furthermore, start to crack the ceramic layer. The time needed for the wave to travel and reflect back is given by

$$t_i = \frac{2e_c}{c_c} + \frac{2e_m}{c_m} \tag{4.1}$$

where e_c and c_c are, respectively, the thickness and the longitudinal velocity of sound for the ceramic material, and e_m and c_m are the same constants for the metallic material.

It is known that the shock wave travels with the longitudinal velocity of sound in the solid, and this velocity can be calculated by

$$c = \sqrt{\frac{E}{\rho}} \tag{4.2}$$

where E is the elastic modulus of the material[15]

The substitution of equation 4.2 in 4.1 gives:

$$t_i = 2e_c\sqrt{\frac{\rho_c}{E_c}} + 2e_m\sqrt{\frac{\rho_m}{E_m}} \qquad 4.3$$

where E_c and E_m are the elastic modulus for the ceramic and metallic material respectively. Equation 4.3 allows a better use of system's properties in the model.

4.2 The Resistance to the Penetration on Ceramic

The simulation for the impact phenomenon must represent the reality by considering experimentally measurable parameters. The present mathematical model is an initial simple approach to the high speed impact situation. The equations of movement and erosion were modeled based on the system properties, considering both bullet and shield materials. However, these equations also involve certain constants, such as R_c and Y_p, that are not usually found experimentally. According to Tate [7] both values represent the pressure that the solid material can support without reaching the hydrodynamic behavior. Tabor [8] also explains that the dynamic yielding Y_p of a metallic material is a function of the velocity of the indentation. Considering the high speed of the impact the same is assumed for the resistance against penetration in the ceramic R_c.

The hardness of a material is measured by different types of indentations in the plane surface of the material. During the low speed indentation test, both plastic and elastic domains act in the resistance of the material. After the removal of the indenter, also in low speed, a material relaxation in the neighborhood of the

indentation hole is expected, which represents the elastic behavior of the material. In the brittle materials this effect is almost absent, but for the ductile materials, such as the material of the bullet, it is an important effect and must be considered in during the experiments or calculations.

In the high speed impact phenomenon the amount of energy per unit of time over the material surface is much higher than in a common indentation process. In this way, the material does not present a full resistance of its elastic domain. Considering this, depending on the velocity of the impact, geometry of the indenter (projectile) and material of both projectile and target bodies, the resistance against penetration or plastic deforming, in the case of the projectile, will be different.

By observing Al-Qureshi's work [1], it is possible to notice that the dynamic yielding Y_p for the projectile material is directly presented. However, the resistances against penetration for the ceramic layer are different for the compositions B and C presented in the literature. Moreover, the same work presents the Vicker's Hardness of both types of ceramics. The values are presented in Table (4.1).

Table 4.1: Vicker's hardness and resistance against penetration in the ceramic for compositions B and C.

	Composition			
	B		C	
Hardness (HV/GPa)	1551.4	15.21	1259.8	12.35
R_c (GPa)	4.43		3.60	

Comparing the presented values, it is possible to notice that

$$\frac{R_{c(b)}}{HV_{(b)}} = \frac{R_{c(c)}}{HV_{(c)}} \tag{4.4}$$

Once the applied load over the surface of the ceramic material is very high and it is done in an extremely short time, even the small plastic or elastic resistances do not fully act during the indentation. Considering this, the presented relation and the Tabor [8] commentaries for the resistance of the materials against penetration by fast indentation, the constant R_c is considered a fraction of the Vicker's hardness of the material.

Then, Tate's equation was modified and a new one is given by:

$$Y_p + \frac{1}{2}\rho_p\left(v(t)-u(t)\right)^2 = 2.84*10^{-3}HV + \frac{1}{2}\rho_c\left(u(t)\right)^2 \tag{4.5}$$

where *HV* is the Vicker's Hardness of the material.

It is important to mention that this modification does not affect the model or the results. This fact also contributes to further experimental tests using this model as basis.

4.3 Metallic Plate Deflection Profile

The metallic layer is responsible for absorbing the remaining energy of the projectile after the second stage. The original mathematical model proposed that the plastic deformation in this plate can be deduced from the effective stress and strain relation. It is given by

$$E_p = \frac{A}{n+1}\int_V \left(\frac{\delta w}{\delta r}\right)^{2(n+1)} dV \qquad 4.6$$

However, the considered profile of deformation $\frac{\delta w}{\delta r}$ and also the considered geometry *dV* for the dimple are simple and could be modified to improve the accuracy of the model.

In the original work, the geometry of a small cylinder for the shape of the dimple after the impact was considered. It was given by

$$dV = 2\pi r h \partial r \,. \qquad 2.3$$

Taking into account that the dimple shape, as shown in Figure 4.1, it can be well represented by the volume of a paraboloid.

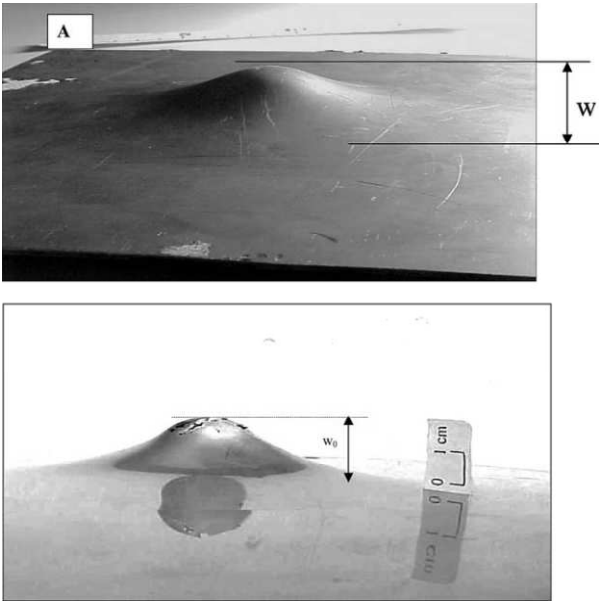

Figure 4.1: Shape of the metallic plate after impact.

The 3D equation of this curve is given by

$$z = x^2 + y^2 \tag{4.7}$$

that has to be transformed to cylindrical coordinates for further steps. It gives

$$z = r^2 \cos\theta^2 + r^2 \sin\theta^2 \tag{4.8}$$

Integrating the curve it is possible to calculate the volume of the solid paraboloid. It is given by

$$V = \int_0^h \int_0^{2\pi} \int_0^r \left(r^2 \cos\theta^2 + r^2 \sin\theta^2\right) dr\, d\theta\, dz \tag{4.9}$$

that becomes

$$V = \frac{2}{3}\pi r^2 h \qquad 4.10$$

In addition, equation 4.9 can be derived to provide the necessary element of volume

$$dV = 2\pi r h \partial r \qquad 4.11$$

The modification in the deformation profile is related to the shape of the curve in the considered parameters.

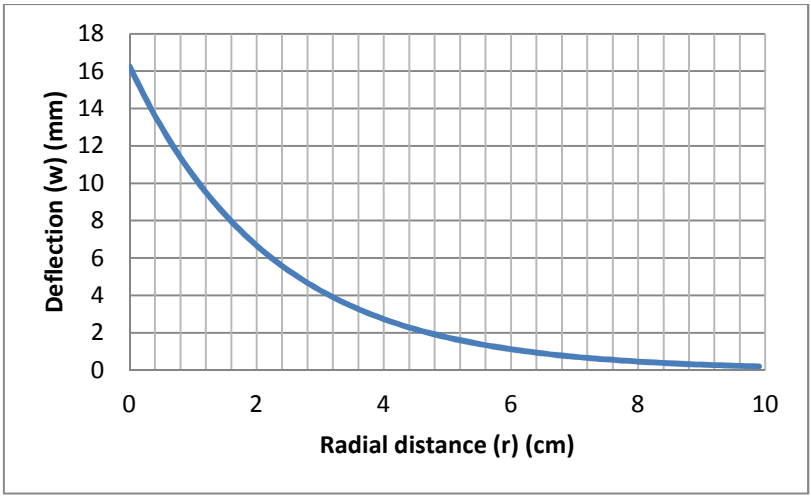

Figure 4.2 Deflection of the metal plate as a function of the radial distance with the original model equations.

The proposed deflection profile is given by

$$w(r) = w_0 e^{\left(-\frac{kr}{d}\right)} \qquad 2.15$$

and with the calculated and given constants (*k* and *d* respectively) the plot of this constant does not fit well, compared to Figure 4.2. The central deformation (in *r* = 0) of the metallic plate is

represented by a sharp edge in Figure 4.2 and the function is not mirrored in the y axis. Considering this, an approach based on the normal distribution curve was done and the modified profile is now given by

$$w(r) = w_0 \, e^{\left(-\frac{k_{\mathrm{mod}} \, r^2}{d}\right)} \tag{4.12}$$

where k_{mod} represents the modified profile constant for the deflection equation. Differentiating the proposed profile it is encountered the necessary term $\frac{\delta w}{\delta r}$ for the plastic energy absorbed by the metallic layer. It is given by

$$\frac{\delta w}{\delta r} = -\frac{2 r k_{\mathrm{mod}}}{d} w_0 e^{\left(-\frac{k_{\mathrm{mod}} \, r^2}{d}\right)} \tag{4.13}$$

By substituting the profile given, by equation 2.15 and also the volume element gave by equation 4.11 in equation 4.6 it is possible to write the modified expression. The simplified equation is given by

$$E_p = \frac{2A\pi h}{n+1}\left(-\frac{2k_{\mathrm{mod}} w_0}{d}\right)^{2(n+1)} \int_0^{\infty} r^{2n+4} e^{\left(-2k_{\mathrm{mod}} r^2 \frac{n+1}{d}\right)} \delta r \tag{4.14}$$

and its solution can be written as

$$E_p = \frac{A\pi h\left(-\frac{2\,k_{\mathrm{mod}}\, w_0}{d}\right)^{2n+2} \Gamma\left(n+\frac{5}{2}\right)\left(\frac{2\,k(n+1)}{d}\right)^{-n-\frac{5}{2}}}{n+1} \tag{4.15}$$

where Γ represents the gamma function.

As same as the original result, it is known that the hardening exponent *n* is fractional (*0 < n < 1*) and this generate a complex value as result of $\left(-\frac{2k_{\text{mod}}\, w_0}{d}\right)^{2n+2}$ because of the negative signal. However, as mentioned in previous chapters, the module of this sentence is considered due to the mirrored y-axis plot of $\frac{\delta w}{\delta r}$, which generates these constants. With this, the sentence becomes

$$E_p = \frac{A\pi h\left(\frac{2k_{\text{mod}}\, w_0}{d}\right)^{2n+2}\Gamma\left(n+\frac{5}{2}\right)\left(\frac{2k_{\text{mod}}(n+1)}{d}\right)^{-n-\frac{5}{2}}}{n+1} \qquad 4.16$$

Considering that the energy absorbed by the plate can be approximately equated to the kinetic energy at the end of the second stage, which is given by

$$E_k = \frac{1}{2}m_{pr}v_{pr}^2 = E_p \qquad 2.22$$

the expression for the maximum deflection of the metal plat can be written as

$$w_0 = \frac{d\left(\frac{1}{2}\frac{m_{pr}v_{pr}^2(n+1)}{A\pi h\Gamma\left(n+\frac{5}{2}\right)\left(\frac{2k_{\text{mod}}(n+1)}{d}\right)^{-n-\frac{5}{2}}}\right)^{\frac{1}{2n+2}}}{2k_{\text{mod}}} \qquad 4.17$$

With this new solution for the metallic plate maximum deformation, it is also necessary to calculate the modified deflection profile constant k_{mod} using the experimental data given by the original work. The same procedure for the constant *k* calculation in the previous chapters has been adopted and the value found for this constant is now $0.0018\ m^{-1}$.

4.4 Comparison to the Modified Duration of First Stage

To compare the modified theory results with the data furnished by Al-Qureshi's work [1], the movement equations had to be once more solved due the new duration of the first stage calculated by equation 4.3. The modified deflection theory was also considered using the constant values given by the same work and the motion input data generated by the movement solution. Moreover, to generate a broader range of comparisons, the solutions were performed using the same composition characteristics and initial velocity data presented in Table 3, given by Al-Qureshi's article as well[1].

Ceramic compositions B and C, mentioned in the article, had different densities and resistance against penetration (related to Vicker's Hardness) which had to be considered in both equation 4.3 and Tate's modified hydrodynamic law 4.5, respectively. To calculate the duration of the first stage, the elastic modulus of 96% pure alumina (Al_2O_3) , given by Accuratus [16], and stainless steel 304 presented by AZoM materials database [17], were considered. The other properties involved in the calculation are shown in Table 4.1.

Table 4.2: Values of the constants used in the modified model.

Symbol	Property	Value
ρ_c	Ceramic Density	*Composition B* $3.9\ g/cm^3$ *Composition C* $3.8\ g/cm^3$
E_c	Ceramic Elastic Modulus	*300 GPa*
e_c	Ceramic Thickness	*11.3 mm* *9.3 mm* *7.3 mm*
R_c	Resistance against penetration on ceramic	*Composition B* *4.43 GPa* *Composition C* *3.60 GPa*
ρ_m	Metal Density	$7.77\ g/cm^3$
E_m	Metal Elastic Modulus	*193 GPa*
e_m **and** h	Metal Thickness	*15 mm*
A	Metal Strength	*935 MPa*
n	Metal Hardening Exponent	*0.29*
K_{mod}	Metal Modified Deflection Profile Constant	$0.0018\ m^{-1}$
Y	Projectile Dynamic Yielding	*2.82 GPa*
ρ_p	Projectile Density	$8.41\ g/cm^3$

Table 4.3 presents the experimental maximum deflection values and also the calculated results and the respective errors considering the old and new theories.

It is possible to note that the new theories presented higher error rate than the old theory results in some of the test. However, the results of the maximum deflection showed that the new theories can generate good results not only for the high speed impacts, but also for lower velocities, differently from the old theory.

Table 4.3: Comparison of the results between the original and modified theories of first stage duration and plastic deformation.

Composition	Thickness (mm)	Duration of the 1st stage (μs)	Impact velocity (m/s)	Maximum Deflection			Errors	
				Experimental Data (mm)	Original Theory OT (mm)	Modified Theories MT (mm)	OT (%)	MT (%)
B	11.3	8.6	792.7	16.5	17.0	17.24	2.9	4.29
C	11.3	8.7	858.2	20.0	17.6	18.38	-13.6	-8.81
B	9.3	8.2	628.9	18.0	17.8	18.8	-1.1	4.25
C	9.3	8.2	651.1	17.5	17.7	18.29	1.1	4.31
B	7.3	7.7	428.8	15.5	17.3	14.62	10.4	-6.01
C	7.3	7.8	448.4	13.0	16.6	13.0	21.7	0

5 SIMULATIONS BASED ON THE MODIFIED THEORIES

The simulations are useful to evaluate the performance of the designed code. In addition, it would be even better to reproduce the simulated phenomena experimentally. However, it was not possible to generate the impact situation in laboratory due to several factors. Considering the bureaucracy and the constraints related to fire weapons and licenses to handle them, it was practically impossible, in this case, to find a person and a place where those tests could be performed in the available time.

The simulations were done to evaluate the effect of the variation of some parameters in the system.

5.1 Simulation on the Thicknesses of the Ceramic Layer

Initially, different thicknesses of the ceramic plate are applied in the program in order to analyze the effect on the absorbed energy, duration of the impact and deformation of the metallic plate. In every simulation it was necessary to keep constant the elastic modulus and density for metal and ceramic in order to vary the ceramic thickness. The values for these constants are presented in Table (4.2) in last section.

The base thickness for the ceramic layer, mentioned by the authors of the original theory [1], was 10 mm. Here, the value is modified by expressing the thickness difference by fractions of the original proposed value. In this way, it is possible to control the thickness of the layer in the program with dimensionless parameters. The selected values to be applied in the code are

50%, 75%, 100% (original), 125% and 150% of the original value proposed by the authors. The aforementioned values are applied into the equation 4.3, from which different time results are obtained for the first stage and, as consequence of this, important consideration about the calculation of the thickness.

The time for the first stage, considering the different thicknesses of the ceramic layer, is presented in Table 5.1.

Figure 5.1 presents the end of the second stage and the final deceleration of the projectile. It is possible to note that the different thicknesses of the ceramic layer do not affect considerably the duration of the phenomenon. Moreover, the same image shows the insignificant differences between the velocities (in the different runs) at the start of the third stage (shift in the curvature). In addition, in the first stage, the different ceramic layers' thicknesses do not affect the duration of this step considerably; it just changes the time between the runs by 0.1 μs.

From this simulation, it is also possible to calculate how much the metal will deflect. The deflection depends on the velocity and the remaining mass by the end of the second stage. For the equation 4.17, most of the values of Table 4.2 were used, except for the remaining mass (m_{pr}) and the velocity in the end of the second stage (v_{pr}). These two values were replaced by the data generated by the simulation. Due to the little difference presented in the simulated results, the metallic layer`s final deflection values were practically the same, presenting differences of 0.1 mm, which were considered negligible.

Table 5.1: Duration of the first stage for different ceramic thicknesses.

Percentage of the original value (10 mm)	Duration of the first stage (μs)
50	7.1
75	7.7
100	8.2
125	8.8
150	9.3

Together with the evolution of the velocity, it is possible to calculate how much the projectile advances into the ceramic during the penetration process, which is described by the second stage equations. This can be easily computed by integrating numerically the projectile velocity data during the second stage. Moreover, by knowing the size of the time intervals (0.1 μs) it can be assumed that the approximation is valid. Table 5.2 presents the advance of the projectile into the ceramic for the different thicknesses used.

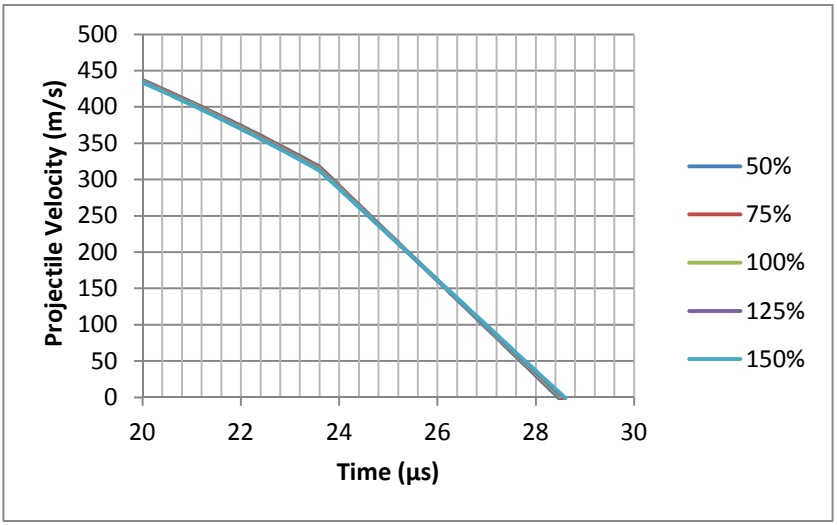

Figure 5.1: evolution of the projectile velocity for different ceramic thicknesses.

It is possible to observe according to Table 5.2 that the two finer ceramic plates are not capable to absorb properly the impact, allowing the projectile to pass through it, compromising the metallic structure. On the other hand, it is obvious that thicker ceramics are not going to be crossed very easily. However, the thickness of the ceramic plate can increase drastically the weight of the whole structure.

Table 5.2: Advance of the projectile in the ceramic tile for different considered plate thicknesses

Thickness of the ceramic plate (mm)	Projectile penetration in the plate (%)
5	179.39
7.5	113.69
10	81.62
12.5	61.86
15	49.21

5.2 Simulation on Different Types of Projectiles

The effect of a bullet impact can be compared to the impact of a high-velocity asteroid (or another solid body in space) in an aerospace protection. This comparison is also valid for the collision between a still body in space and an aircraft travelling at high speed. This second round of simulations is based on different types of projectiles. The model has to show clear responses for the different geometries and masses of the projectile, otherwise it will not be omnivalent and all the equations will have to be changed for the different numerical parameters inserted.

The geometry data used for the projectiles are from the National Institute of Justice Standards (USA) – Ballistic Resistance of Body Armor [18]. The literature classifies the

different types of body armor by the specifications of each bullet`s type and velocity. It would take a long time if all the different parameters were used in the simulation. Then, one or two parameters for each type of protection were used. Table 5.3 shows the projectiles` data that were used.

Table 5.3: Parameters used in the simulation for different type of projectiles.

Type	Specification	Bullet Diameter (mm)	Mass (g)	Initial Velocity (m/s)
II	.357 Magnum	10,2	10,2	453
IIA	9 mm	9	8	373
IIA	.40S&W	10,2	12	300
IIIA	.357 SIG	9,02	8,1	440
IIIA	.44 Magnum	10,9	16	460

From the input parameters presented in Table 5.3, it is possible to run the simulations and plot the velocity evolution graph for the different types of projectiles. This graph is shown in Figure 5.2

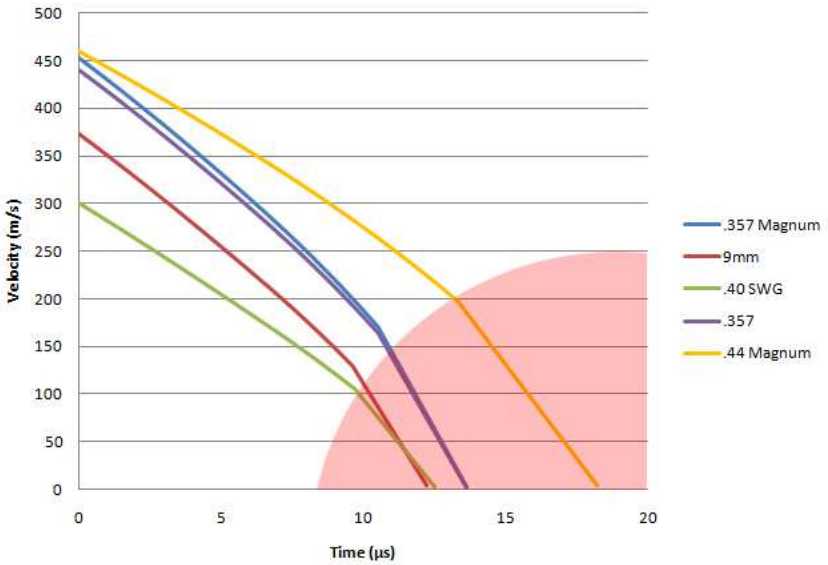

Figure 5.2: Velocity(m/s) versus time(s) for the different parameters of mass, diameter and initial velocity of the projectiles.

As known, the shift in the curvatures demonstrates the end of the second stage for every simulation. At this point, the velocity of the interface, which is not shown in the above plot, is equal to the bullet velocity. The marked region in the graph corresponds to the probable area of velocity and time where the erosion does not occur. This helps to investigate the effect of the ceramic`s characteristics in the impact absorption and in the erosion. This graph and this model of simulation can be used to search for specific properties in the ceramic plate and/or to improve its shock absorption property.

Similarly to the simulation on the different ceramic thicknesses, it is possible to calculate the final deflection of the

metal plate. Using the velocity and the mass at the end of the second stage for each simulation plus the constants` data given by Table 4.2, the deflection values for each type of projectile together with the percentage of advance inside the ceramic layer are shown in Table 5.4.

Table 5.4: Values of final deflection and penetration in the ceramic layer

Type	Specification	Velocity (m/s)	Mass (g)	Deflection Value (mm)	Penetration in the Ceramic (%)
II	.357 Magnum	170	6.66	19.48	87.5
IIA	9mm	129	5.80	18.71	41.4
IIA	.40S&W	104	9.45	18.63	49.6
IIIA	.357 SIG	163	5.36	17.40	84.4
IIIA	.44 Magnum	197	10.38	20.15	90.1

In Table 5.4, it is possible to notice that the mass of the projectile is also another important factor in the impact. Heavier projectiles tend to penetrate more in the protection and deform more the metallic back plate, as expected. However, the low velocity of the projectile imposes also low erosion rates to the projectile, which loses lower amounts of mass.

5.3 Simulation on the Metal Layer Properties

Another important part of the protection is the back metal plate, which is responsible for the absorption of the final kinetic energy. The characteristics of this metal can determine if the protection will fail or not. Considering this, a deterministic simulation was made based on the equation 4.17 together with equation 4.12, which gives

$$w(r) = \frac{d\left(\frac{1}{2}\frac{m_{pr}\,v_{pr}^{2}\,(n+1)}{A\pi h\Gamma\left(n+\frac{5}{2}\right)\left(\frac{2k_{\mathrm{mod}}\,(n+1)}{d}\right)^{-n-\frac{5}{2}}}\right)^{\frac{1}{2n+2}}}{2k_{\mathrm{mod}}} \times e^{\left(-\frac{k_{\mathrm{mod}}\,r^{2}}{d}\right)} \qquad 5.1$$

In this equation, it is possible to find two constants plus the radial distance value (*r*) that can be changed at will. Those are the dimensionless constant *n* and the thickness of the plate *h*. Moreover, the value of another mechanical property of the metal *A* could be modified, but the result would be similar to the variation in the thickness *h* of the material.

Figure 5.3 presents the surface plot of the maximum deformation as a function of *r* and *n* and Figure 5.4 presents the same deflection in function of *h* and *r.*

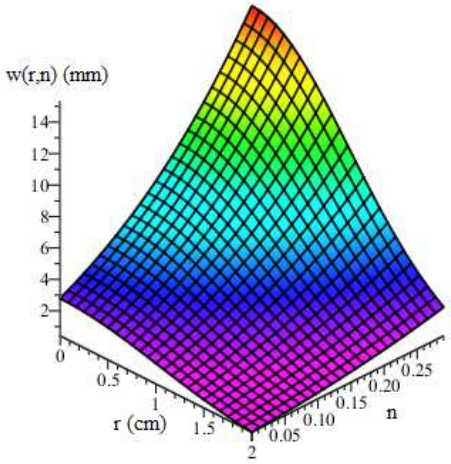

Figure 5.3: Deformation *w* in function of the radial distance *r* and the hardening exponent *n.*

Based on Figures 5.3 and 5.4, it is possible to affirm that the mechanical property *n* and the thickness *h* of the metal layer have an important effect on the maximum deflection. The *n* constant demonstrates the ductile behavior of the material. However, if a lower deflection is required, it is important to note that a harder material could shear more easily depending on the energy of the projectile. Moreover, a change in the thickness of the metal plate will certainly affect the structure weight, which could be an aggravating factor in the carrier's mobility.

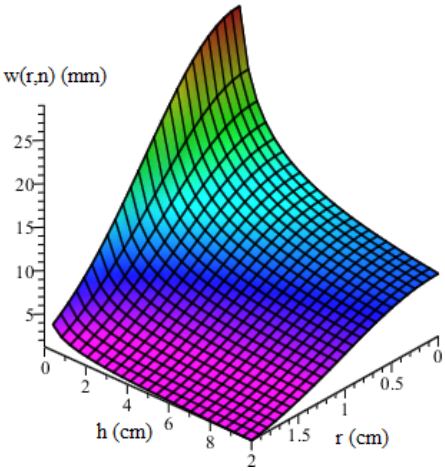

Figure 5.4: Deflection of the metallic plate *w* in function of the metal thickness *h* and radial distance *r.*

6 CONCLUSIONS

6.1 Concluding Remarks

The model has proved to be reliable to represent the impact of a colliding bullet on a ceramic-metal system. However, the proposed equations and stages are a simplification of a complex phenomenon, which is the high speed impact. The results and comparison presented in the tables and graphs validated the model in its original solution, even not considering several side effects that can affect drastically the experimental results. In addition, the modified equations could approximate the results with the experimental data presented in the literature by preventing the behavior of the system even in impacts with lower velocity.

In addition, the simulation demonstrated different aspects of the model and some predictable effects in collision phenomena. The control of the properties and its effects were analyzed with the developed computational method. Some of the effect predicted by the program could not be studied experimentally. However, future studies can use the presented results to validate the theory and, then, analyze some internal phenomena in a deeper way.

6.2 Future Studies

The presented work is a theoretical analysis of the impact phenomenon in a specified type of protection. In the future studies, the current model, its solutions and simulations can be used to perform experimental test to evaluate the reliability of the model. Also, if the model can be considered valid for the impact, the considerations and formulations can be kept or improved to a more advanced modeling as FEM (finite element modeling). In addition, the experimental confirmation of the presented modeling also permits deeper investigations of the impact phenomenon, such as the effect of the interfacial friction between the projectile and sheared surfaces.

Moreover, in a partnership with Construções Mecânicas Cocal LTDA., which leads a project of armor development, the presented study will be improved and used as a resource to investigate the effects of the collision in the already developed armor prototype involving ceramic, polymeric and metallic materials.

7 REFERENCES

1. AL-QURESHI, H. A.; GONÇALVES, D. P.; DE MELO, F. C. L.; KLEIN, A. N. Analysis and investigation of ballistic impact on ceramic/metal. **International Journal of Machine Tools & Manufacture**, p. 307–316, 2004.
2. IQBAL, M. A.; GUPTA, N. K. Energy absorption characteristics of aluminum plates subjected to. **Latin American Journal of Solids and Structures**, p. 259 - 287.
3. JERZ, J.; SIMANčÍK, F.; BORTEL, M.; KUBO, S.; KOVÁčIK, J. The Design of Lightweight Armour Sheets. **Cellular Metals and Metal Foaming Technology**, 2003.
4. NAIK, N. K.; SHRIRAO, P. Composite Structures Under Ballistic Impact. **Composite Structures**, p. 579–590, 2004.
5. VANICHAYANGKURANONT, T.; CHOLLACOOP, N.; MANEERATANA, K. **Numerical Simulation of Ballistic Impact on Ceramic Armor**. 4th Thailand Materials Science and Technology Conference. 2006.
6. SILVA, P. H. F.; KAJITA, T.; GONÇALVES, D. P.; MELO, F. C. L. **Desenvolvimento de Vitro-Cerâmicas de Alta Resistência ao Impacto com**

Aplicações em Blindagens Balísticas. 17º CBECIMat - Congresso Brasileiro de Engenharia e Ciência dos Materiais. 2006.

7. TATE, A. A Theory for the Deceleration of Long Rods After Impact. **J. Mech. Phys. Solids**, p. 387 - 399, 1967.

8. TABOR, D. **The Hardness of Metals**, 1951.

9. WILKINS, M. L. Mechanics of penetration and perforation. **Int. J. Eng. Sci.**, p. 793 - 807, 1978.

10. WILKINS, M. L. Use of Boron Compounds in Lightweight Armor. **Boron and refractory borides**, p. 633, 1977.

11. KOZHUSHKO, A. A.; RYKOVA, I. I.; SINANI, A. B. Resistance of Ceramic To Projectile Penetration at High Interaction Velocities. **Fizika Goreniya i Vzryva**, Leningrad, v. 28, p. 89-93, 1990.

12. HILL, R. **The Mathematical Theory of Plasticity**. Oxford University Press, 1950.

13. AL-QURESHI, H. A.; BRESSAN, J. D. **9th The North Manufacturing Research Conf**. Investigation of the Degree of Biaxiality on the Limit Strains in Sheet Metal Stretching. 1981. p. 538 - 541.

14. AL-QURESHI, . A.; ISHIKURA, D. **Physical Metallurgy and Materials Science Conference**

on Advanced Materials and Technology. Study of Perforation of Metals and Composite Materials Plates by Projectile. Kraków-Krynica: 1998. p. 544-547.

15. HALLIDAY, D.; RESNICK, R.; WALKER, J. **Fundamentals of Physics**. 4. ed., v. 2.

16. **Accuratus**. Disponivel em: <http://accuratus.com/alumox.html>. Acesso em: 2011.

17. **Azom Materials**. Disponivel em: <http://www.azom.com/article.aspx?ArticleID=965>. Acesso em: 2011.

18. U.S. DEPARTMENT OF JUSTICE, N. I. O. J. **Ballistic Resistance of Body Armor, NIJ Standard–0101.06**., 2008.

8 PUBLICATION

The following articles were developed and submitted along the research work devoted to this dissertation:

NECKEL,L.; HOTZA,D.; STAINER,D.; JANSSEN,R.; LEZANA,A.G.R.; DIAS,A.; AL-QURESHI, H.A. Solutions for Impact over Aerospace Protection. **Key Engineering Materials.** Vols. 488-489 (2012) pp 25-28.